Russian Academy of Sciences
Joint Institute for High Temperatures RAS
Institute of Problems of Chemical Physics RAS
Kabardino-Balkarian State University

Physics of Extreme States of Matter — 2014

Moscow, 2014

Physics of Extreme States of Matter — 2014

Edited by academician Fortov V. E., Karamurzov B. S., Efremov V. P., Khishchenko K. V., Sultanov V. G., Levashov P. R., Andreev N. E., Kanel G. I., Iosilevskiy I. L., Mintsev V. B., Petrov O. F., Savintsev A. P., Shakhray D. V., Shpatakovskaya G. V.

This compendium is devoted to investigations in the fields of thermal physics of extreme states of matter and physics of high energy densities. Different models and results of theoretical calculations of equations of state for materials at high pressures and temperatures, physics of shock, detonation and combustion waves, interaction of intense laser, x-ray and microwave radiation, powerful particle beams with matter, techniques of intense energy fluxes generation, experimental methods of diagnostics of ultrafast processes, low-temperature plasma physics, issues of physics and power engineering, as well as technology projects are considered. The majority of the works has been presented at the XXIX International Conference on Equations of State for Matter (March 1–6, 2014, Elbrus, Kabardino-Balkaria, Russia). The edition is intended for specialists in physical and technical problems of power engineering.

This conference is dedicated to the centenary of birth of academician Yakov Borisovich Zel'dovich (March 8, 1914–December 2, 1987).

The conference is sponsored by the Russian Academy of Sciences and the Russian Foundation for Basic Research (grant No. 13-02-06212).

The editorial board announces with deep regret the death of the colleagues and friends, Dr. Vladimir Vladimirovich Milyavskiy (July 22, 1969–June 12, 2013), who was the organizing and program committees member of the Conferences on Equations of State for Matter and Interaction of Intense Energy Fluxes with Matter, and Prof. Gennady Vasil'evich Sin'ko (February 7, 1950–September 8, 2013), who was a regular and active participant of these conferences starting with one of the first meeting.

ISBN 978-5-94691-625-7

CONTENTS

CHAPTER 1. EQUATIONS OF STATE FOR MATTER

CHAPTER 2. SHOCK WAVES. DETONATION. COMBUSTION

CHAPTER 3. POWER INTERACTION WITH MATTER

CHAPTER 4. PHYSICS OF LOW TEMPERATURE PLASMA

POWER INTERACTION WITH MATTER

FROZEN NANOSTRUCTURES PRODUCED BY ULTRASHORT LASER PULSE

***Khokhlov V. A.*[1]*, *Inogamov N. A.*[1], *Anisimov S. I.*[1], *Zhakhovsky V. V.*[2], *Emirov Yu. N.*[3], *Ashitkov S. I.*[2], *Komarov P. S.*[2], *Agranat M. B.*[2]**

[1]*ITP RAS, Chernogolovka,* [2]*JIHT RAS, Moscow,* [3]*AMERI FIU, Miami, United States*

**V_A_Kh@mail.ru*

Surface nanostructures, arising under the influence of a short laser pulse on a metal target as a result of nucleation, stretching and then freezing of foam-like material in the surface melt, are considered.

Keywords: Short pulse laser ablation, surface nanostructures, frozen nanofoam

Introduction. When we speak of the surface structures arising under laser irradiation, the first thing that usually comes to mind is a regular ripple-like structure arising from the interaction of the incident and surface electromagnetic waves. The properties of such structures are defined by the resonance condition between the incident and surface waves. Further, such structures will not be considered.

We will study irregular structure, the cause of which, as a rule, is the development of thermal and hydrodynamic inhomogeneities. A typical representative of such structures is a foam-like structures remaining on the surface of the target after a short laser pulse.[1]

Experimental results [1]. In the described experiments the study of deformation of the target surface in the area, heating by femtosecond (100 fs) pulse (FLP) of Cr:forsterite laser system, was performed using femtosecond interference microscopy.[2] There is a crater on the target surface after exposure in the case if laser fluence in spot center F_c exceedes ablation threshold F_{abl}. Fig. 1 shows an example of the crater interferogram at $F_c > F_{abl}$. The structure of the surface layer

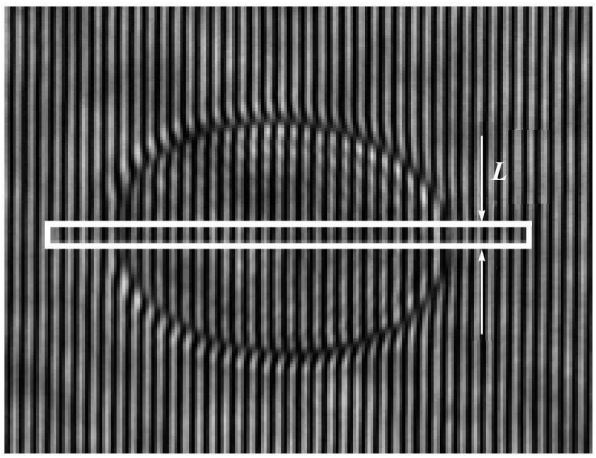

Figure 1. Interferogram of the ablation crater on the surface of an aluminum target after exposure to FLP. Rectangle shows a face of the membrane which was cut by the electron beam (schematically, not to scale vertically, the membrane thickness is $L = 150$ nm)

of the target with a residual deformation was investigated by Transmission Electron Mitcroscopy (TEM) by preparing a thin membrane (shown schematically in Fig. 1, which is then analyzed by a transmission microscope Technai TF 20. As a result there the existence of nanocavities observed inside deformed surface layer, Fig. 2

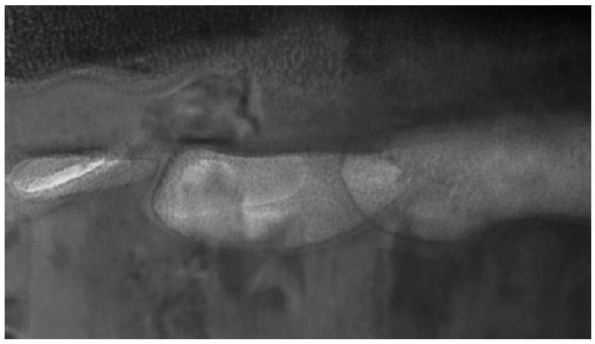

Figure 2. Subsurface structure of an aluminum target with nanocavities, which were formed from the cavitation bubbles ensemble during the freezing of the melt. The image of the membrane plane on TEM is shown.

2T stage. Fast heating of electrons by short laser pulse converts the metal in two-temperature (2T) state with the electron temperature T_e is much greater than the ion (phonoh) temperature T_i. An underlying concept of 2T state of metal with hot electrons and cold ions was suggested in the paper [3]. To solve 2T heat conduction equations the accurate values of an electron-ion coupling parameter α [4–6] and electron heat conduction $\kappa, \chi = \kappa/c_e$ [5–7] are required, here c_e is electron heat capacity. The required data have been obtained from solutions of kinetic equations in τ-approximation [6, 7]. Reliable description of the 2T conduction is necessary since $\kappa_{2T} \sim 10^3$ WK^{-1}m^{-1} is very high (far beyond $\kappa_{1T} \sim 100$ WK^{-1}m^{-1}) and κ together with α defines thermal depth $d_T \sim \sqrt{\chi_{2T} t_{eq}}$ ~ 100 nm. Thus d_T turns out few times larger than an optical skin depth $\delta \approx$10-20 nm.[8] Here $t_{eq} \sim c_i/\alpha$ $\sim 2 - 10$ ps is an electron-ion temperature equilibration time, ion heat capacity $c_i \approx 3k_B n_{atom}$, $\alpha \sim 10^{17}$ WK^{-1}m^{-3} [4, 6], $d_T \sim v_F\sqrt{t_{eq}\tau_e}$, $\tau_e = 1/\nu_e$, where v_F is Fermi velocity, $\nu_e = \nu_{ei} + \nu_{ee}$ is electron collision frequency.

Within a 2T stage, which lasts t_{eq}, the speed of heat propagation (thermal wave) is very large $v_{th} \sim c_s(v_F/c_s)\sqrt{\tau_e/t}$ because Fermi velocity v_F and its Mach number are large $\mathrm{Ma}_F = v_F/c_s \sim 100$. For flu-

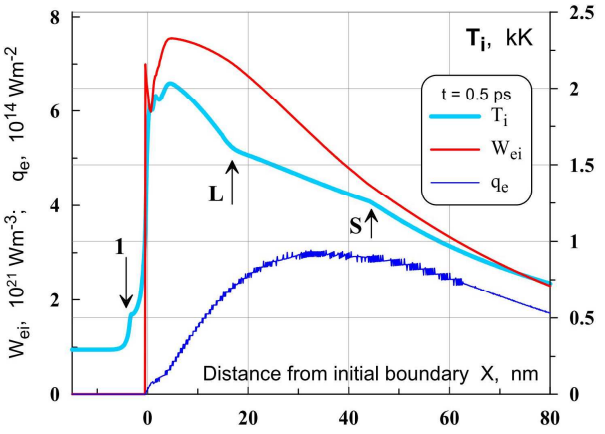

Figure 3. Spatial distributions of temperatures of ion subsystem T_i, electron thermal flux q_e taken with inverse sign, and power of electron-ion energy transfer W_{ei} per unit of volume. Al film was irradiated from the left side through a glass substrate. Initially glass was at $x < 0$, Al film was placed $0 < x < 1.2$ um. Laser pulse has duration $\tau_L = 100$ fs, time is reckoned from a maximum of a pulse, energy $F_{abs} = 0.13$ J/cm^2 is absorbed in a skin layer of $\delta = 15$ nm. Arrow 1 marks shock in glass. We neglect light absorption and heat conductivity in glass. Therefore, the ion heating W_{ei} decreases sharply at the glass-Al interface.

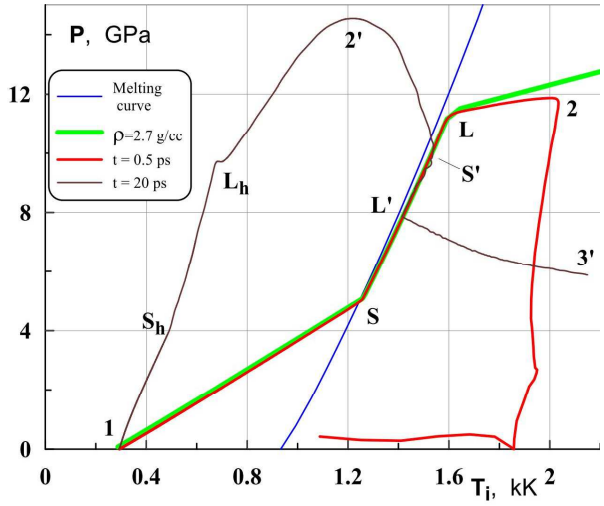

Figure 4. Melting and isochoric curves of Al together with profiles at 2T ($t = 0.5$ ps) and hydrodynamic ($t = 20$ ps) stages. The end point 3' sits inside a melt. Its position is $x = 95$ nm ($t = 20$ ps). The T, p values for inner melt and glass ($x < 95$ nm) are not shown for $t = 20$ ps.

ences near and higher than the ablation threshold F_{abl}, which is few times higher than melting threshold F_m, the velocity of melting front v_m is also large $v_m \sim v_{th}$. It should be noted that for such a case it is not possible to utilize the Stefan problem for estimation of heat penetration in the 2T stage. Indeed, 2T system cannot provide a finite heat flux (into solid) concentrated in the *point* M, where M is an instantaneous melting front position in Stefan problem approximation, because energy release via electron-ion energy transfer $W_{ei} = \alpha\,(T_e - T_i)$ is spatially distributed and therefore the electron heat flux $q_e = \kappa(\partial T_e/\partial x)$ is continuous, see Fig. 3. In Stefan problem the melting zone tightens into a propagating point M where a jump of thermal flux $\{\kappa T_x\}$ supplies energy necessary for melting of solid in a point M moving with finite velocity $v_m = \{\kappa T_x\}/\rho\lambda$, where λ is latent heat of fusion per unit mass, ρ is density of solid prior to influx into point M. Figure 3 shows result from hydrodynamic simulation including 2T heat balances and elastic properties of solid. Arrows "L" and "S" give instant positions of liquidus "L" and solidus "S". On the thermodynamic phase diagram they bound solid-liquid mixture zone. Outside the mixture zone the electron-ion local energy flux W_{ei} is spent only for heating of ions. While inside the zone the flux is spent for heating of mixture *simultaneously* with expenses going to increase fraction of liquid in mixture. Therefore, the T_i profile has kinks on liquidus "L" and solidus "S".

Let's call the front "L" marked in Fig. 3 as a melting front, because there is pure liquid to the left side relative to this point. At a moment shown in Fig. 3 the front velocity is 63 km/s! This is hypersonic velocity, therefore, liquid do not have time to decrease its density after melting (isochoric regime), and ion pressure increases during fast heating (expansion release is too slow at this time scale). This is a reason why the melting temperatures T_i in points "L" and "S" in Fig. 3 are higher than the triple point temperature 0.934 kK for Al. Profiles of thermo-mechanical flow on the phase plane $T - p$ are shown in Fig. 4. Within the 2T stage at $t = 0.5$ ps the profile 1-S-L-2 is almost coincide with a curve corresponding to initial density of Al. The point 1 gives a room temperature state of Al far from glass-Al boundary. The points S and L present solidus and liquidus, as in Fig. 3. Maximum of T_i (the point 2 in Fig. 4) is achieved near a glass-Al boundary, see Fig. 3. Dependence $p_i(T_i)$ at $t = 0.5$ps is shown as the profile 1-S-L-2 in Fig. 4. This curve can be presented also in a parametric form: $T_i(x)$, $p_i(x)$. Near a boundary the density of Al drops due to expansion in direction of glass. At this early stage the expansion of Al is driven mainly by electron pressure p_e.

Spatial positions of point S and L at pressure p_i and temperature T_i profiles in Figs. 3 and 4 coincide during supersonic propagation of heat. Images of those points on pressure profile in the hydrodynamic "h" stage are marked as L_h and S_h in Fig. 4. The "h" stage follows the 2T stage. At the "h" stage those images are split off from their positions in 2T stage - comp. L_h, S_h versus L, S in Fig. 4. The images propagate along acoustic characteristics carrying values of pressure corresponding to isochoric melting. But temperatures in points L_h and S_h decrease during propagation because the points move to the right along the x axis, as shown in Fig. 3, and temperature decreases in this direction. As a results, a gap between the (L_h, S_h) and (L, S) line segments is formed on the $T - p$ plane. We refer to this process as emission of compression wave by decelerating thermal wave.

Let's mention also an inverse behavior of ion temperature between points S' and L' in Fig. 4. The points S' and L' belong to a melting curve but not to an isochoric curve, see Fig. 5. Distribution of thermodynamic parameters along the spatial profile inter-

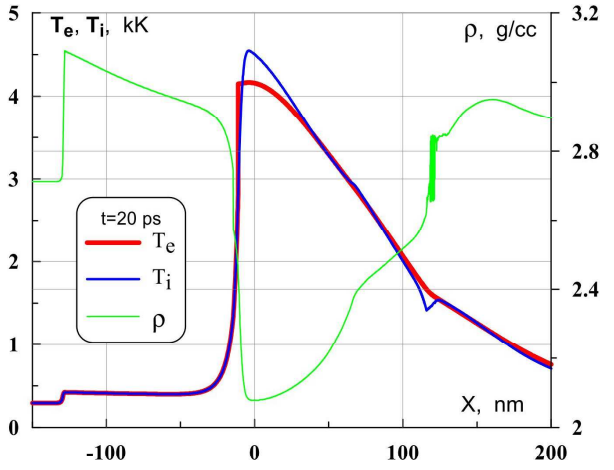

Figure 5. Layer of molten Al near glass-Al boundary. Electrons transfer energy from a hot place and therefore become colder than ions in this hot place. This picture is interesting since it shows how the 2T case $T_e \gg T_i$ tends to a limit where description through Stefan task becomes valid in metals: $c_e/c_i \ll 1$, $\kappa_e/\kappa_i \gg 1$.

sects a two-phase solid-liquid melting zone along differently directed line segments on a thermodynamic phase plane. On a $\rho - T$ plane those segments rotate from isochoric to isobaric directions during transition from 2T to 1T flow. The feature with inverse dependence of T_i in Fig. 5 isn't connected with mechanical reasons - namely, with a release of shear stress in a melting zone. It also exists in the pure plastic hydrodynamic simulations, see Fig. 5 in [8]. This feature is linked to the finite heat of fusion and expenses of energy on melting. Small deviations from exact local equilibration $T_e = T_i$ remains in 1T stage, see Fig. 5. They are necessary for thermal transport from hot to cold places, because ion heat capacity c_i is larger than electron capacity c_e while heat in metals is carried mainly by electrons (ratio of thermal diffusivities χ_i/χ_e is small).

Resolidification and surface nano-structures Time scales of thermal and hydrodynamic processes taking place in a surface layer of target are: $t_{eq} \sim 2-7$ ps – duration of 2T stage; $t_{hd} \sim 20$ ps – hydrodynamic stage; t_{st} – stopping of motion near surface; and $t_{sol} \sim 1$ ns – solidification of molten metal. For fluences higher than the nucleation threshold $F > F_{nucl}$ [1] the scale t_{st} increases sharply from small values $\sim t_{hd}$ to a nanosecond time scale. This is caused by large difference in rigidity between continuous melt and foam-like material. In case with bubbles the near surface velocities drop down to $\sim 10 - 100$ m/s for $F > F_{nucl}$ and $t \sim 1$ ns. Thus, t_{st} becomes $\sim t_{sol}$ and situations with freezing of slowly moving nanostructures may realize [1]. The corresponding picture of frozen bubbles beneath the surface obtained in molecular dynamics (MD) simulation [9, 10] is shown in Fig. 6.

A result of analysis a wide range of MD calculations for different levels of pumping energy they can be devided into three qualitatively different segments: (i) $F < F_{nucl}$, (ii) $F_{nucl} < F < F_{abl}$ and (iii) $F_{abl} < F$.

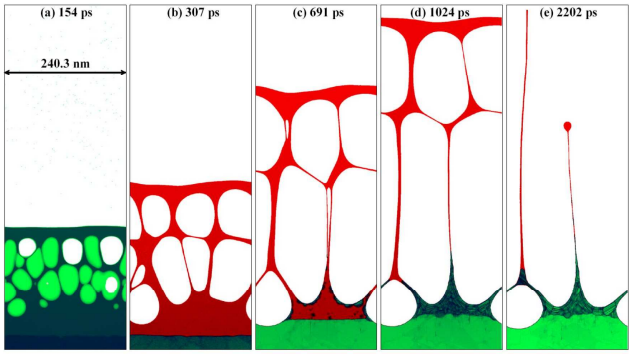

Figure 6. Expansion and freezing of foamed aluminum. As a result of electron cooling of molten surface layer the resolidification front moves up through continuous melt and reaches the bottoms of bubbles. Due to supercooling of surface liquid at later time, solid nuclei are also formed inside the melt and at free surface. (a) cavitation in liquid surface layer shown on density map; (b-e) atomic order parameter shows phase state of material: green colors correspond to solid state, while red colors correspond to liquid; (c) crystallization begins at liquid-solid interface first, then in bulk of supercooled melt and at free boundary of melt; (d) crystallization of foam walls initiated by formation of solid nuclei on free liquid surfaces of walls; (e) liquid walls are broken, a tiny droplet forms at the end, and liquid jet moves back to the target along partially frozen pike.

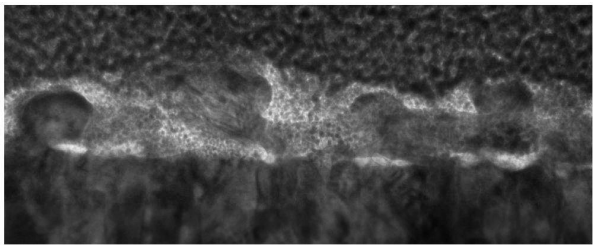

Figure 7. Focused ion beam/transmission electron microscopy (FIB/TEM, lamella technique) cut of nickel surface. The lamella has been taken from a lateral part of a crater produced by a single optical laser shot. The grey layer on the top is a protecting layer of Pt organic. Dark knobs are frozen jets. Bright crescent are deformed frozen nanobubbles similar to the bubbles observed in Al target, see Fig. 2

In case (ii) "frozen foam" can be observed, see Fig. 7

In the paper [1] fluence corresponds to the case (iii), in the central region of the laser spot and the case (ii) on the periphery.

In the case (iii) we call such structures "frozen broken foam".

Such structures is obtained also with X-ray lasers [11, 12]. In the X-ray case the plasmonic effects are negligible. Therefore, the X-ray structures remain chaotic (no ripples) after any number of laser shots N. The performed experiments confirm this.

Optical lasers produce similar structures [13–17]. Our analysis shows that they appear if $F > F_{nucl}$ and $N \sim 1$.

This is a key explaining thermo-mechanical mechanism of appearance of chaotic surface nano-structures. The existence of similar structures and a wide range

of wavelengths of laser from the optical to the X-ray confirms their thermo-mechanical fluctuation nature.

Acknowledgements. This work was supported by the RAS program "Substance with high energy density" and RFBR grant 13-08-01095-a.

1. Ashitkov S. I., Inogamov N. A., Zhakhovsky V. V., Emirov Y. N., Agranat M. B., Oleinik I. I., Anisimov S. I. & Fortov V. E. Formation of Nanocavities in Surface Layer of Aluminum Target irradiated by Femtosecond Laser Pulse // JETP Lett., 2012. V. 95. P. 176-181. [Pis'ma v ZhETF. 2012. V. 95 P. 192-197]
2. Agranat M. B., Andreev N. E., Ashitkov S. I., Veisman M. E., Levashov P. R., Ovchinnikov A. V., Sitnikov D. S., Fortov V. E. & Khishchenko K. V. Determination of the transport and optical properties of a nonideal solid-density plasma produced by femtosecond laser pulses // JETP Lett., 2007. V. 85. P. 271-276. [Pis'ma v ZheTF. 2007. V. 85. P. 328-333]
3. Anisimov S. I., Kapeliovich B. L., & Perel'man T. L. Electron emission from metal surfaces exposed to ultrashort laser pulses. // Sov. Phys. JETP. 1974. V. 39 P. 375–377. [ZhETF. 1974. V. 66. P. 776-779]
4. Lin Z., Zhigilei L. V., & Celli V. Electron-phonon coupling and electron heat capacity of metals under conditions of strong electron-phonon nonequilibrium. // Phys. Rev. B. 2008. V. 77. P. 075133.
5. Amoruso S., Bruzzese R.,Wang X., & Atanasov P. A.. Femtosecond laser ablation of nickel in vacuum. // J. Phys. D.: Appl. Phys. 2007. V. 40. P. 331-340.
6. Petrov Yu. V. , Inogamov N. A., & Migdal K. P. Thermal conductivity and the electron-ion heat transfer coefficient in condensed media with a strongly excited electron subsystem. // JETP Letters. 2013. V. 97. P. 20-27. [Pis'ma v ZheTF. 2013. V. 97. P. 24-31]
7. Petrov Yu. V. and Inogamov N. A. Elimination of the Mott Interband s-d Enhancement of the Electrical Resistance of Nickel and Platinum Owing to the Excitation of Electrons by Femtosecond Laser Pulses. // JETP Lett. 2013. V. 98 P. 278-284. [Pis'ma v ZheTF. 2013. V. 98. P. 316-322]
8. Inogamov N. A., Ashitkov S. I., Zhakhovsky V. V., Shepelev V. V., Khokhlov V. A., Komarov P. S., Agranat M. B., Anisimov S. I., & Fortov V. E. Acoustic probing of two-temperature relaxation initiated by action of ultrashort laser pulse. // Appl. Phys. A. 2010. V. 101. P. 1-5.
9. Inogamov N. A., Zhakhovsky V. V., Petrov Yu. V., Khokhlov V. A., Ashitkov S. I., Khishchenko K. V.,. Migdal K. P, Ilnitsky D. K., Emirov Yu. N., Komarov P. S., Shepelev V. V., Miller C. W., Oleynik I. I., Agranat M. B., Andriyash A. V., Anisimov S. I., & Fortov V. E. Electron-ion relaxation, phase transitions, and surface nano-structuring produced by ultrashort laser pulses in metals. // Contributions to Plasma Physics. 2013. V. 53 N. 10. P. 796-810.
10. Inogamov N. A., Zhakhovsky V. V., Petrov Y. V., Khokhlov V. A., Ashitkov S. I., Migdal K. P., Ilnitsky D. K., Emirov Y. N., Khishchenko K. V. Komarov P. S., Shepelev V. V., Agranat M. B. Anisimov S. I., Oleynik I. I. & Fortov V. E. Ultrashort laser - matter interaction at moderate intensities: two-temperature relaxation, foaming of stretched melt, and freezing of evolving nanostructures // SPIE Proceedings. 2013. V. 9065. P. 906502,1-14
11. Ishino M., Faenov A. Ya., Tanaka M., Hasegawa N., Nishikino M., Tamotsu S., Pikuz T. A., Inogamov N. A., Zhakhovsky V. V., Skobelev I. Yu., Fortov V. E., Khohlov V. A., Shepelev V V., Ohba T., Kaihori T., Ochi Y., Imazono T., & Kawachi T. Nanoscale surface modifications and formation of conical structures at aluminum surface induced by single shot exposure of soft x-ray laser pulse. // J. Appl. Phys. 2011. V. 109 P. 013504.
12. Ishino M., Faenov A. Ya., Tanaka M., Hasegawa N., Nishikino M., Tamotsu S., Pikuz T. A., Inogamov N. A., Zhakhovsky V. V., Skobelev I. Yu., Fortov V. E., Khohlov V. A., Shepelev V. V., Ohba T., Kaihori T., Ochi Y., Imazono T., & Kawachi T. Interaction of soft x-ray laser pulse radiation with aluminum surface: Nano-meter size surface modification. // AIP Conference Proceedings. 2012. V. 1465. P. 236-240.
13. Vorobyev A. Y. and Guo Ch Reflection of femtosecond laser light in multipulse ablation of metals. // J. Appl. Phys. 2011. V. 110. P. 043102,1-9.
14. Hashida M., Ikuta Y., Miyasaka Y., Tokita S., & Sakabe S. Simple formula for the interspaces of periodic grating structures self-organized on metal surfaces by femtosecond laser ablation. // Appl. Phys. Lett. 2013. V. 102. P. 174106.
15. Savolainen J.-M., Christensen M. S., & Balling P. Material swelling as the first step in the ablation of metals by ultrashort laser pulses. // Phys. Rev. B. 2011. V. 84. P. 193410.
16. Gurevich E. L. Self-organized nanopatterns in thin layers of superheated liquid metals. // Phys. Rev. E. 2011. V. 83. P. 031604,1-5.
17. Ionin A. A., Kudryashov S. I., Makarov S. V., Seleznev L. V., Sinitsyn D. V., Ligachev A. E, Golosov E. V., & Kolobov Y. R. Sub-100 nanometer transverse gratings written by femtosecond laser pulses on a titanium surface. // Laser Phys. Lett. 2013. V. 10. P. 056004.